Novel Method for Detection of Genes With Altered Expression Caused by Coronavirus Infection and Screening of Candidate Drugs for SARS-CoV-2

Y-H. Taguchi and Turki Turki

***Abstract*—To better understand the genes with altered expression caused by infection with the novel coronavirus strain SARS-CoV-2 causing COVID-19 infectious disease, a tensor decomposition (TD)-based unsupervised feature extraction (FE) approach was applied to a gene expression profile dataset of the mouse liver and spleen with experimental infection of mouse hepatitis virus, which is regarded as a suitable model of human coronavirus infection. TD-based unsupervised FE selected 134 altered genes, which were enriched in protein-protein interactions with orf1ab, polyprotein, and 3C-like protease that are well known to play critical roles in coronavirus infection, suggesting that these 134 genes can represent the coronavirus infectious process. We then selected compounds targeting the expression of the 134 selected genes based on a public domain database. The identified drug compounds were mainly related to known antiviral drugs, several of which were also included in those previously screened with an *in silico* method to identify candidate drugs for treating COVID-19.**

***Index Terms*—COVID-19, SARS-CoV-2, *in silico* drug discovery, gene expression profile, tensor decomposition, feature extraction**

I. Introduction

THE current pandemic of COVID-19 caused by infection of the new coronavirus strain SARS-CoV-2 is a severe public health problem that must be resolved as soon as possible. To achieve this goal, it is essential to understand the mechanism by which SARS-CoV-2 successfully invades human cells. Recently, Pfaender et al. [1] demonstrated that host lymphocyte antigen 6 (LY6E) complex impairs coronavirus fusion and confers immune control of viral disease. The authors also used a transcriptome approach to evaluate the effect of infection of mouse hepatitis virus (MHV), a natural mouse pathogen that causes hepatitis and encephalomyelitis, which is a well-studied model of coronavirus infection. Although they found many pathways that were disturbed after MHV infection, they did not perform a detailed analysis of the genes with altered expression in response to MHV infection.

In this study, we applied tensor decomposition (TD)-based unsupervised feature extraction (FE) [2] to identify genes with altered expression by MHV infection as a model of coronavirus. We further performed functional enrichment on the selected genes to determine their potential associations with coronavirus infection processes, and screened candidate drug compounds targeting these genes. Overall, this work expands TD formalism by exploring the interpretation of six-dimensional tensors in an infectious disease context. Moreover, we demonstrate a novel application of TD to facilitate the drug discovery process, which can offer a valuable resource for researchers to obtain mechanistic insight for identifying effective drugs for infectious diseases such as COVID-19.

Y-H. Taguchi is with the Department of Physics, Chuo University, Tokyo 112-8551, Japan, e-mail:tag@granular.com (see https://researchmap.jp/Yh_Taguchi/).

Turki Turki is with the Department of Computer Science, King Abdulaziz University, Jeddah 21589, Saudi Arabia

II. Materials and Methods

A. Gene expression profile dataset

The gene expression profile was downloaded from the Gene Expression Omnibus (GEO) dataset GSE146074. This dataset comprises the gene expression profiles of the liver and spleen from female mice experimentally infected with MHV or injected with phosphate-buffered saline (PBS) as a control group for comparison. This experiment was performed with mice of two genetic backgrounds, including wild-type (WT) mice and an textit Ly6e-knockout (KO) mutant strain. The number of replicates for each group are listed in Table I.

TABLE I
NUMBER OF BIOLOGICAL REPLICATES. TWO TECHNICAL REPLICATES ARE AVAILABLE FOR EACH BIOLOGICAL REPLICATE.

	PBS day 5		MHV day 3		MHV day 5	
	liver	spleen	liver	spleen	liver	spleen
WT	3	3	3	3	3	3
KO	3	3	3	3	3	3

B. TD-based unsupervised FE

The gene expression profile dataset was formatted as a tensor, $x_{ijkmnp} \in \mathbb{R}^{N\times 2\times 2\times 3\times 3\times 2}$, which represents the expression level of the ith gene of the jth genotype ($j = 1$:KO, $j = 2$:WT) of the kth tissue ($k = 1$:liver, $k = 2$:spleen) of the mth treatment group ($m = 1$:PBS day 5, $m = 2$:MHV day 3, $m = 3$:MHV day 5) for the nth biological replicate ($1 \le n \le 3$) and pth technical replicate ($1 \le p \le 2$).

The TD is therefore expressed as

$$\begin{aligned} x_{ijkmnp} &= \sum_{\ell_1\ell_2\ell_3\ell_4\ell_5\ell_6} G(\ell_1\ell_2\ell_3\ell_4\ell_5\ell_6) \\ &\times u_{\ell_1 j} u_{\ell_2 k} u_{\ell_3 m} u_{\ell_4 n} u_{\ell_5 p} u_{\ell_6 i} \end{aligned} \quad (1)$$

where $G(\ell_1\ell_2\ell_3\ell_4\ell_5\ell_6) \in \mathbb{R}^{N\times 2\times 2\times 3\times 3\times 2}$ is a core tensor, and $u_{\ell_1 j} \in \mathbb{R}^{2\times 2}$, $u_{\ell_2 k} \in \mathbb{R}^{2\times 2}$, $u_{\ell_3 m} \in \mathbb{R}^{3\times 3}$, $u_{\ell_4 n} \in \mathbb{R}^{3\times 3}$,

Preprints (www.preprints.org) | NOT PEER-REVIEWED | Posted: 24 April 2020 doi:10.20944/preprints202004.0431.v1

TABLE II
$G(1,1,2,1,1,\ell_5)$S COMPUTED BY THE HOSVD ALGORITHM

ℓ_5	$G(1,1,2,1,1,\ell_5)$	ℓ_5	$G(1,1,2,1,1,\ell_5)$
1	-11.846381	6	22.375546
2	-28.104674	7	-41.997092
3	312.362569	8	-9.048416
4	-71.001444	9	9.212773
5	-189.719321	10	3.394629

$u_{\ell_5 p} \in \mathbb{R}^{2\times 2}$, and $u_{\ell_6 i} \in \mathbb{R}^{N\times N}$ are singular values vectors, which can be obtained via the higher-order singular value decomposition (HOSVD) algorithm [2].

To select $u_{\ell_6 i}$, attributed to selected genes, we need to select $u_{\ell_1 j}$ attributed to the genotype, $u_{\ell_2 k}$ attributed to the tissue, $u_{\ell_3 m}$ attributed to the treatment, $u_{\ell_4 n}$ attributed to the biological replicate, and $u_{\ell_5 p}$ attributed to the technical replicate, associated with desired properties.

For this study, we sought to identify genes whose expression is independent of the mouse genotype, tissue type, and replicate. Thus, $u_{\ell_1 j}$, $u_{\ell_2 k}$, $u_{\ell_4 n}$, and $u_{\ell_5 p}$ should be independent of j, k, n, and p.

By contrast, we require $u_{\ell_3 m}$ to be dependent on $u_{\ell_3 1} < u_{\ell_3 2} < u_{\ell_3 3}$ or vice versa. This is because $m = 2$ (3 days after MHV infection) must be between $m = 1$ (5 days after PBS injection as the control) and $m = 3$ (5 days after MHV infection).

After selecting $\ell_1, \ell_2, \ell_3, \ell_4$, and ℓ_5 based on the above considerations, we selected ℓ_6 associated with $G(\ell_1\ell_2\ell_3\ell_4\ell_5\ell_6)$ as the largest absolute value, with fixed $\ell_1, \ell_2, \ell_3, \ell_4$, and ℓ_5 values. Using the selected $u_{\ell_6 i}$, The P-values, P_is, were attributed to gene expression levels as

$$P_i = P_{\chi^2}\left[> \left(\frac{u_{\ell_6 i}}{\sigma_{\ell_6}}\right)^2 \right] \tag{2}$$

where $P_{\chi^2}[> x]$ is the cumulative probability distribution of the χ^2 distribution when the argument is larger than x and σ_{ℓ_6} is the standard deviation of $u_{\ell_6 i}$.

P_is were adjusted by the Benjamini and Hochberg criterion [2], and only genes associated with an adjusted P_i less than 0.01 were selected for further analysis.

C. Enrichment analysis

Gene symbols of genes selected by TD-based unsupervised FE with significantly altered expression due to MHV infection were uploaded to Enricher [3] and Metascape [4], which are popular enrichment analysis servers that evaluate the biological properties of genes based on enrichment analysis.

III. RESULTS

A. Selection of genes

We selected $\ell_1 = 1, \ell_2 = 1, \ell_3 = 2, \ell_4 = 1$, and $\ell_5 = 1$ based on the criteria described above (Fig. 1), and the associated $G(1,1,2,1,1,\ell_5)$ values are listed in Table II, demonstrating the largest value for $G(1,1,2,1,1,3)$. The associated P_i values were computed using u_{3i} as shown in eq. (2), resulting in selection of 134 genes altered in MHV infection with adjusted P-values less than 0.01 (Table III). Although some mouse-specific genes were included in this list (e.g., genes with symbols starting with "mt"), since there were still several gene symbols that are common between human and mice, we decided to evaluate the potential association of all 134 genes with the infection process of coronavirus.

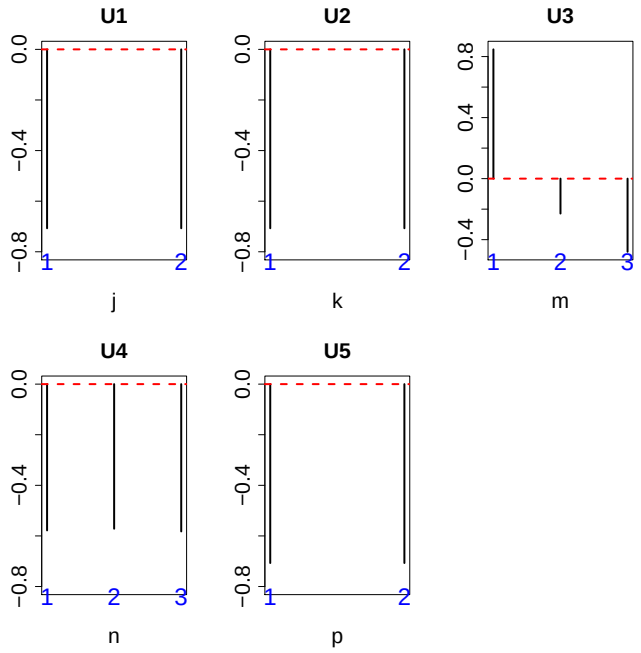

Fig. 1. Singular value vectors obtained by the HOSVD algorithm. U1:U_{1j}, U2:U_{1k}, U3:U_{2m}, U4: U_{1m}, and U5:U_{1p}. See Materials and Methods for the meanings of $j, k, m, n, andp$.

TABLE III
ONE HUNDRED AND THIRTY FOUR GENES SELECTED BY TD-BASED UNSUPERVISED FE

Actb Actg1 Ahsg Alb Ambp Apoa1 Apoa2 Apoc1 Apoe B2m Bst2 C3 Ccnb1ip1 Cd74 Cfb Eef1a1 Eef1g Eef2 Fabp1 Fau Fga Fgb Fgg Fth1 Ftl1 Gapdh Gc Gm10800 Gm2000 Gpx1 H2-Aa H2-D1 H2-K1 H2-T23 Hamp Hba-a2 Hbb-bs Hbb-bt Hist1h3b Hist1h4h Hist2h2aa2 Hp Hpx Hsp90ab1 Hsp90b1 Hspa8 Ifi27l2a Ifitm3 Lars2 Lcn2 Lyz2 mt-Atp6 mt-Atp8 mt-Co1 mt-Co2 mt-Co3 mt-Cytb mt-Nd1 mt-Nd2 mt-Nd3 mt-Nd4 Mt1 Mt2 Myh9 Orm1 Orm2 Pabpc1 Psap Ptma Rack1 Rpl10-ps3 Rpl11 Rpl12 Rpl13 Rpl13a Rpl14 Rpl17 Rpl19 Rpl23a Rpl26 Rpl3 Rpl32 Rpl36 Rpl36a Rpl37a Rpl38 Rpl4 Rpl41 Rpl5 Rpl6 Rpl7 Rpl7a Rpl8 Rplp0 Rplp1 Rplp2 Rps11 Rps12 Rps14 Rps15 Rps17 Rps18 Rps2 Rps21 Rps23 Rps24 Rps27a Rps27rt Rps29 Rps3 Rps3a1 Rps4x Rps5 Rps6 Rps7 Rps8 Rps9 Rpsa S100a8 S100a9 Saa1 Saa2 Serpina1a Serpina1b Serpina1c Serpina1d Serpina3k Tmsb4x Tpt1 Trf Ttr Ubb Ubc Wfdc21

B. Protein-protein interaction with coronavirus infection

We first evaluated whether the 134 selected genes could reflect the process of coronavirus infection using the Enrichr server for functional enrichment analysis. Several of the genes were enriched in the category "Virus-Host PPI P-HIPSTer 2020", which is related to SARS-CoV (Table IV, see the supplementary materials for the full list).

These genes were also related to ORF1ab, polyprotein, and 3C-like protease. Interestingly, Woo et al. [5] suggested

TABLE IV
SARS-CoV-related virus PPI in Enrichr

Term	Overlap	P-value	Adjusted P-value
SARS coronavirus excised_polyprotein 1..4369 (gene: orf1ab)	10/194	7.52×10^{-7}	1.68×10^{-3}
SARS coronavirus P2 full_polyprotein 1..4382	10/198	9.06×10^{-7}	1.01×10^{-3}
SARS coronavirus nsp7-pp1a/pp1ab (gene: orf1ab)	4/36	9.61×10^{-5}	2.08×10^{-2}
SARS coronavirus 3C-like protease (gene: orf1ab)	3/19	2.63×10^{-4}	3.05×10^{-2}

that ORF1ab, which encodes a replicase polyprotein of CoV-HKU1, is cleaved by papain-like proteases and 3C-like proteinase. Thus, it is reasonable that ORF1ab, polyprotein, and 3C-like protease would be affected during MHV infection IV. Other PPIs detected that are not listed in Table IV (see supplementary materials) were also mainly associated with ORF1ab and polyproteins, suggesting that our strategy has clear capability to elucidate the basic infectious process at the molecular level that is common among various coronaviruses.

C. Virus perturbation

We next evaluated whether genes with known altered expression by virus perturbation overlapped with the 134 genes selected by our TD-based unsupervised FE approach (Table V; see the supplementary material for the full list).

Among these, we detected the overlap of many genes that are pertubated in response to either SARS-CoV or SARS-like bat CoV, which are the genetically closest coronaviruses to the new SARS-CoV-2 strain. This further suggests that our results could have high similarity to the genes perturbated in SARS-CoV-2 infection.

D. TMPRSS2 as a scavenger receptor

For further functional enrichment analysis, we uploaded the 134 selected genes to Metascape to identify non-redundant biological terms (Fig. 2). Among the terms identified, "R-HSA-2173782: Binding and Uptake of Ligands by Scavenger Receptors" was the third most significantly enriched term. Although it was initially surprising that a scavenger receptor might be related to the response to coronavirus infection, a search of the related literature revealed that the scavenger receptor TMPRSS2 plays a critical role in SARS-CoV-2 infection as well as SARS-CoV infection [6]. Isolation of SARS-CoV-2 was also reported to be enhanced by TMPRSS2-expressing cells [7]. Moreover, TMPRSS2 contains a scavenger receptor domain [8], suggesting that TMPRSS2 activity would be related to detection of scavenger receptor activity. This finding further demonstrates the outstanding capability of our strategy to detect factors related to the SARS-CoV-2 infectious process. Moreover, this analysis suggests that research on the SARS-CoV infection process could be informative for understanding the SARS-CoV-2 infection process when it is not possible to directly investigate SARS-CoV-2 infection.

E. Drug discovery

We previously demonstrated that genes selected by TD-based unsupervised FE are useful to screen for drugs that are effective in treating disease or those that may cause adverse effects [9]. Therefore, we used this approach to screen for candidate drugs to treat coronavirus infections based on the individual terms that emerged from the Enrichr analysis.

1) Drug Matrix: In the Enrichr category "DrugMatrix", the top-ranked drug was related to virus infection (Table VI; see the supplementary materials for the full list). Most of these viruses are enveloped, single-stranded RNA viruses. Coronaviruses, including SARS-CoV-2, are positive-sense, enveloped, single-stranded RNA viruses, whereas influenza virus is a negative-sense, enveloped, single-stranded RNA virus.

Primaquine is known to inhibit the replication of Newcastle disease virus [10], which is in the family of paramyxoviruses that are enveloped, non-segmented, negative-sense single-stranded RNA viruses. Meloxicam is known to have cytotoxic and antiproliferative activity on virus-transformed tumor cells [11], including myelocytomatosis virus and Rous sarcoma virus. Myelocytomatosis virus is a retrovirus, which is an enveloped, negative-sense, single-stranded RNA virus, whereas Rous sarcoma virus is an enveloped, positive-sense, single-stranded RNA virus. Although there are no studies showing that cytarabine is effective against infection of an RNA virus, one report demonstrated that cytarabine can affect DNA virus infection [12]. Pyrogallol was reported to have anti-virus effects on human influenza virus strain A/Udorn/72, avian influenza virus A/swan/Shimane/499/83, herpes simplex virus-1, vesicular stomatitis virus, and retrovirus [13]. As mentioned above, influenza virus is a negative-sense, enveloped, single-stranded RNA virus; herpesvirus is a DNA virus; vesicular stomatitis virus is an enveloped, single-stranded, negative-sense RNA virus; and retroviruses are enveloped, negative-sense, single-stranded RNA viruses. This suggests that a single drug can effectively inhibit a wide range of viruses from DNA viruses to both negative- and positive-sense RNA viruses. The structure-dependent antiviral activity of catechol derivatives in pyroligneous acid against encephalomyocarditis virus was reported, which is a non-enveloped single-stranded RNA virus [14]. To our knowledge, there are no reports that neomycin is effective against RNA viruses; however, one study showed that it could inhibit infection of fibroblasts with human cytomegalovirus [15], which is a DNA virus.

Although not all viruses identified to be related to the 134 genes selected by TD-based unsupervised FE are enveloped, positive-sense, single-stranded RNA viruses similar to SARS-CoV-2, since drugs shown to be effective against other viruses (e.g., DNA viruses) are also often effective against RNA viruses (including pyrogallol that was screened by our strategy), drugs in Table VI warrant being tested as potential treatments for SARS-CoV-2 infection.

2) Drug Perturbations from GEO: Several promising drug compound candidates were also screened from the GEO "Drug

Preprints (www.preprints.org) | NOT PEER-REVIEWED | Posted: 24 April 2020 doi:10.20944/preprints202004.0431.v1

TABLE V
VIRUS PERTURBATION IN ENRICHER

Term	Overlap	P-value	Adjusted P-value
up			
SARS-ddORF6 24Hour GSE47961	10/300	3.52×10^{-5}	3.79×10^{-3}
cSARS Bat SRBD 60Hour GSE37827	9/300	1.93×10^{-4}	1.04×10^{-2}
SARS-BatSRBD 60Hour GSE47961	8/300	9.51×10^{-4}	4.38×10^{-2}
down			
SARS-BatSRBD 96Hour GSE47960	11/300	5.77×10^{-6}	4.66×10^{-4}
SARS-BatSRBD 84Hour GSE47960	9/300	1.93×10^{-4}	6.24×10^{-3}
cSARS Bat SRBD 60Hour GSE37827	8/300	9.51×10^{-4}	2.36×10^{-2}

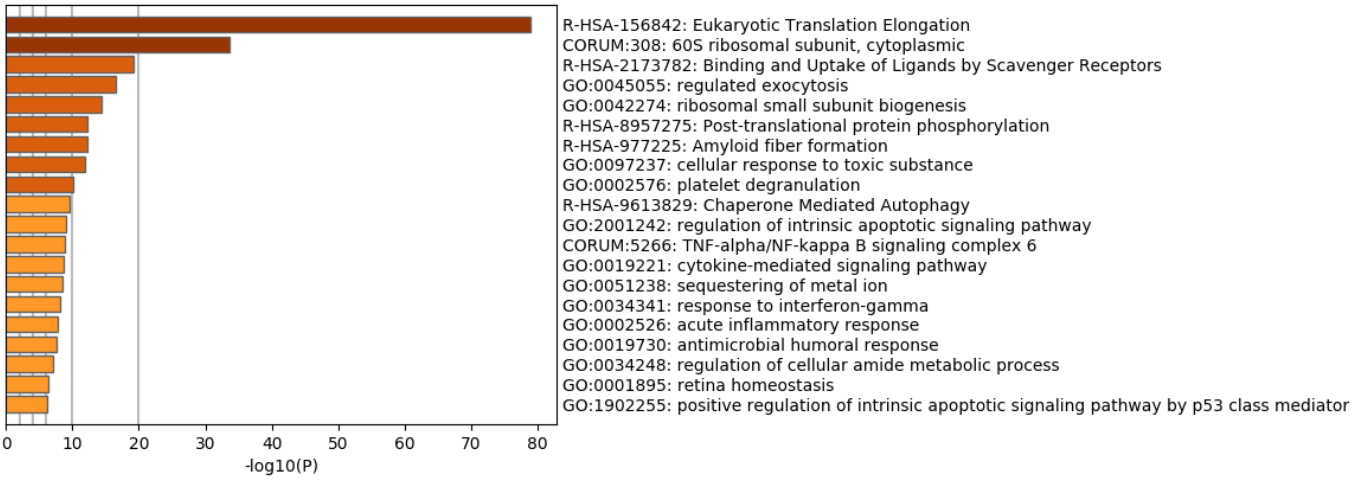

Fig. 2. Redundant heatmap of enriched terms generated by uploading the selected 134 genes to Metascape

TABLE VI
DRUGS ENRICHED IN THE "DRUGMATRIX" CATEGORY IN ENRICHR. THE FULL LIST IS AVAILABLE IN THE SUPPLEMENTARY MATERIAL

Term	Overlap	P-value	Adjusted P-value
Primaquine-45 mg/kg in CMC-Rat-Liver-5d-up	23/315	1.40×10^{-17}	1.10×10^{-13}
Meloxicam-33 mg/kg in Corn Oil-Rat-Kidney-1d-up	23/337	6.19×10^{-17}	2.44×10^{-13}
Cytarabine-487 mg/kg in Saline-Rat-Liver-0.25d-up	22/300	6.87×10^{-17}	1.80×10^{-13}
Clotrimazole-60 uM in DMSO-Rat-Primary rat hepatocytes-0.67d-dn	24/381	7.59×10^{-17}	1.49×10^{-13}
Diclofenac-3.5 mg/kg in Corn Oil-Rat-Liver-5d-dn	21/269	1.04×10^{-16}	1.64×10^{-13}
Pyrogallol-1000 mg/kg in Water-Rat-Liver-3d-up	23/349	1.33×10^{-16}	1.75×10^{-13}
Clindamycin-161 mg/kg in Saline-Rat-Kidney-1d-up	23/366	3.76×10^{-16}	4.23×10^{-13}
Catechol-195 mg/kg in Saline-Rat-Liver-0.25d-up	21/290	4.76×10^{-16}	4.69×10^{-13}
Anisindione-75 mg/kg in CMC-Rat-Liver-5d-up	21/295	6.72×10^{-16}	5.88×10^{-13}
Phenylhydrazine-78 mg/kg in Water-Rat-Liver-3d-up	22/335	7.00×10^{-16}	5.51×10^{-13}
N-Nitrosodiethylamine-1.67 mg/kg in Saline-Rat-Liver-0.25d-up	23/377	7.15×10^{-16}	5.12×10^{-13}
Neomycin-56 mg/kg in Corn Oil-Rat-Liver-1d-dn	20/259	7.28×10^{-16}	4.78×10^{-13}

Perturbations from GEO up" and "Drug Perturbations from GEO down" categories, along with available evidence for possible adverse effects (Table VII; see the supplementary material for the full list).

Drugs associated with upregulated genes that overlapped with the 134 genes selected by TD-based unsupervised FE are considered to be more likely to cause adverse effects, since they will enhance the expression of genes altered by SARS-CoV infection. Captoprilis is an angiotensin-converting enzyme (ACE) inhibitor, which is known to activate ACE2 that is the receptor that SARS-CoV-2 uses to infect human cells [16], suggesting that this drug might have negative effects for COVID-19 therapy. Coenzyme Q10, which frequently emerged in Table VII, has been reported to accelerate virus infection [17], which could therefore also have negative effects for COVID-19 therapy. Fenretinide is known to effectively inhibit HIV infection [18], and therefore might be a promising drug candidate for SARS-CoV-2 even though it was listed in the "Drug Perturbations from GEO up" category.

In contrast to the drugs in the above list, those associated with downregulated genes that overlapped with the 134 genes selected by TD-based unsupervised FE are considered to be able to effectively suppress SARS-CoV-2 infection, since they will inhibit the expression of genes altered by SARS-CoV infection. Pioglitazone was also included in the list of candidate compounds for SARS-CoV-2 screened by an *in silico* method [19]. Quercetin was reported to inhibit the cell entry of SARS-CoV-2 [20], and was also included in

 doi:10.20944/preprints202004.0431.v1

TABLE VII
DRUGS IDENTIFIED IN "DRUG PERTURBATIONS FROM GEO UP/DOWN" IN ENRICHR FOR THE 134 GENES SELECTED BY TD-BASED UNSUPERVISED FE.

Term	Overlap	P-value	Adjusted P-value
Drug Perturbations from GEO up			
coenzyme Q10 5281915 mouse GSE15129 sample 3464	64/302	1.32×10^{-81}	1.20×10^{-78}
coenzyme Q10 5281915 mouse GSE15129 sample 3456	63/396	1.05×10^{-71}	4.78×10^{-69}
captopril DB01197 mouse GSE19286 sample 2689	47/134	1.76×10^{-70}	5.33×10^{-68}
ubiquinol 9962735 mouse GSE15129 sample 3463	60/346	2.28×10^{-70}	5.15×10^{-68}
N-METHYLFORMAMIDE 31254 rat GSE5509 sample 3570	56/283	8.87×10^{-69}	1.61×10^{-66}
1-Naphthyl isothiocyanate 11080 rat GSE5509 sample 3568	56/301	3.80×10^{-67}	5.73×10^{-65}
fenretinide 5288209 rat GSE3952 sample 3561	59/397	6.98×10^{-65}	9.04×10^{-63}
coenzyme Q10 5281915 mouse GSE15129 sample 3462	50/257	1.49×10^{-60}	1.69×10^{-58}
bexarotene DB00307 human GSE6914 sample 2680	43/147	3.03×10^{-60}	3.05×10^{-58}
FENRETINIDE 5288209 rat GSE3952 sample 3563	52/345	5.99×10^{-57}	5.42×10^{-55}
Drug Perturbations from GEO up			
pioglitazone DB01132 rat GSE21329 sample 2841	56/321	1.85×10^{-65}	1.67×10^{-62}
quercetin DB04216 mouse GSE38067 sample 3441	59/486	1.81×10^{-59}	8.19×10^{-57}
ubiquinol 9962735 mouse GSE15129 sample 3461	53/349	2.64×10^{-58}	7.95×10^{-56}
fenretinide 5288209 rat GSE3952 sample 3559	56/440	2.31×10^{-57}	5.21×10^{-55}
decitabine 451668 mouse GSE4768 sample 3108	45/226	1.06×10^{-54}	1.91×10^{-52}
troglitazone DB00197 rat GSE21329 sample 2832	50/355	4.51×10^{-53}	6.79×10^{-51}
adenosine triphosphate 5957 human GSE30903 sample 3219	49/341	2.16×10^{-52}	2.78×10^{-50}
alitretinoin DB00523 rat GSE3952 sample 2673	53/483	1.54×10^{-50}	1.74×10^{-48}
bexarotene 82146 rat GSE3952 sample 3560	48/361	1.42×10^{-49}	1.43×10^{-47}
HYPOCHLOROUS ACID 24341 human GSE11630 sample 3201	41/221	2.67×10^{-48}	2.41×10^{-46}
streptozocin DB00428 mouse GSE38067 sample 3439	44/287	4.40×10^{-48}	3.61×10^{-46}
rosiglitazone DB00412 mouse GSE35011 sample 2813	44/290	7.13×10^{-48}	5.36×10^{-46}
motexafin gadolinium (4 h) DB05428 human GSE2189 sample 3125	43/302	1.70×10^{-45}	1.18×10^{-43}

the list of candidate compounds for SARS-CoV-2 screened by an *in silico* method [21]. Fenretinide was also included in the drugs identified as effective compounds in the "Drug perturbations from GEO up" category as described above. Decitabine is one of the drugs used in HIV combination therapy [22]. Troglitazone impedes the oligomerization of sodium taurocholate co-transporting polypeptide and entry of hepatitis B virus into hepatocytes [23], which is a partially double-stranded DNA virus. Finally, motexafin gadolinium was reported to selectively induce apoptosis in HIV-1-infected CD4+ T helper cells [24].

Based on these observations, our strategy appears to be useful to identify potential drug compounds for SARS-CoV-2.

F. Comparison with in silico drug discovery

Finally, we compared the drugs screened out using our approach from the "Drug perturbations from GEO up/down" lists with those screened from two *in silico* drug discovery studies [19], [21]

1) Comparison with Wu et al. [19]: We found multiple hits, which are summarized in Table VIII. The main drugs identified included doxycycline, ascorbic acid, isotretinoin, pioglitazone, cortisone, and tibolone.

Wu et al. [19] identified 29 potential PLpro inhibitors, 27 potential 3CLpro inhibitors, and 20 potential RdRp inhibitors from the ZINC drug database, and identified 13 potential PLpro inhibitors, 26 potential 3Clpro inhibitors, and 20 Potential RdRp inhibitors from their in-house natural product database. Doxycycline was among both the potential PLpro and 3CLpro inhibitors; ascorbic acid and isotretinoin were among the potential PLpro inhibitors; pioglitazone was among the potential 3CLpro inhibitors; and cortisone and tibolone were included in the potential RdRp inhibitors from the ZINC drug database. These multiple hits also further support the suitability of our strategy.

2) Comparison with Ubani et al. [21]: Ubani et al. [21] screened a library of 22 phytochemicals with antiviral activity obtained from the PubChem database for activity against the spike envelope glycoprotein and main protease of SARS-CoV-2. Among these, we found only one hit that overlapped with our screened out drugs, which was quercetin (Table IX).

IV. DISCUSSION AND CONCLUSION

In this paper, we present a novel evaluation method to identify drugs that could be used to effectively treat COVID-19. We applied a TD-based unsupervised FE method to select genes with altered expression caused by MHV infection in mice. Although the dataset analyzed for this study was not based on SARS-CoV-2 infection, the 134 genes selected by TD-based unsupervised FE can still be considered useful for gaining a better understanding of the infectious mechanism of SARS-CoV-2 for several reasons. First, the 134 genes selected were enriched in general RNA virus proteins that play important roles during infectious processes. This suggests that the infectious mechanism represented by the 134 genes in the mouse model is also applicable to SARS-CoV-2 infection. In fact, these genes were also enriched in processes related to scavenger receptor activity, which might reflect the critical role of TMPRSS2 activity in SARS-CoV-2 replication, suggesting a potential therapeutic target.

Following these achievements, we tried to identify potential drug candidate compounds that could influence the 134 selected genes. Among these, we screened out several candidate compounds that are known antiviral drugs, including those that were screened out as drug candidate compounds for SARS-CoV-2 using *in silico* methods.

TABLE VIII
LIST OF *in silico* SCREENED DRUGS [19] WHOSE TARGET GENES WERE ALSO ENRICHED IN THE 134 GENES SELECTED BY TD-BASED UNSUPERVISED FE.

Term	Overlap	P-value	Adjusted P-value
Drug Perturbations from GEO up			
doxycycline DB00254 mouse GSE29848 sample 3209	32/267	3.73×10^{-31}	3.56×10^{-30}
doxycycline DB00254 human GSE2624 sample 3074	28/175	6.59×10^{-31}	6.22×10^{-30}
doxycycline DB00254 human GSE2624 sample 3077	27/209	3.34×10^{-27}	2.46×10^{-26}
doxycycline DB00254 human GSE2624 sample 3076	25/272	1.71×10^{-21}	8.32×10^{-21}
doxycycline DB00254 mouse GSE29848 sample 3207	22/225	1.40×10^{-19}	6.10×10^{-19}
doxycycline DB00254 mouse GSE29848 sample 3208	12/291	6.24×10^{-07}	1.40×10^{-06}
ascorbic acid 54670067 human GSE11919 sample 3190	8/313	1.25×10^{-3}	2.33×10^{-3}
isotretinoin DB00982 human GSE10432 sample 2772	8/308	1.13×10^{-3}	2.11×10^{-3}
pioglitazone DB01132 rat GSE21329 sample 2843	48/400	2.31×10^{-47}	7.49×10^{-46}
pioglitazone DB01132 rat GSE21329 sample 2842	42/349	3.21×10^{-41}	6.19×10^{-40}
pioglitazone DB01132 rat GSE21329 sample 2842	42/349	3.21×10^{-41}	6.19×10^{-40}
pioglitazone DB01132 rat GSE20219 sample 2794	13/292	8.57×10^{-08}	2.01×10^{-07}
pioglitazone 4829 mouse GSE1458 sample 2587	11/318	1.00×10^{-05}	2.13×10^{-05}
pioglitazone DB01132 mouse GSE32536 sample 2797	7/307	4.69×10^{-3}	8.40×10^{-3}
pioglitazone DB01132 rat GSE20219 sample 2795	7/330	6.90×10^{-3}	1.22×10^{-2}
hydrocortisone DB00741 human GSE7890 sample 2751	40/305	1.01×10^{-40}	1.75×10^{-39}
tibolone 444008 human GSE12446 sample 3204	15/287	9.26×10^{-10}	2.38×10^{-9}
Drug Perturbations from GEO down			
doxycycline DB00254 human GSE2624 sample 3075	20/358	3.39×10^{-13}	1.34×10^{-12}
doxycycline DB00254 mouse GSE29848 sample 3208	17/309	2.91×10^{-11}	1.02×10^{-10}
doxycycline DB00254 human GSE2624 sample 3077	18/391	1.37×10^{-10}	4.58×10^{-10}
doxycycline DB00254 mouse GSE29848 sample 3207	17/375	5.85×10^{-10}	1.86×10^{-09}
doxycycline DB00254 human GSE2624 sample 3074	17/425	3.88×10^{-09}	1.16×10^{-08}
doxycycline DB00254 mouse GSE29848 sample 3209	9/333	4.16×10^{-04}	8.91×10^{-04}
ascorbic acid 54670067 human GSE11919 sample 3190	19/287	6.71×10^{-14}	2.75×10^{-13}
Ascorbic acid 54670067 mouse GSE37676 sample 3132	15/306	2.23×10^{-9}	6.89×10^{-9}
pioglitazone DB01132 rat GSE21329 sample 2841	56/321	1.85×10^{-65}	1.67×10^{-62}
pioglitazone 4829 mouse GSE1458 sample 2587	28/282	5.89×10^{-25}	5.26×10^{-24}
pioglitazone DB01132 rat GSE20219 sample 2794	25/308	3.62×10^{-20}	2.25×10^{-19}
pioglitazone DB01132 rat GSE20219 sample 2795	21/270	1.12×10^{-16}	5.41×10^{-16}
pioglitazone DB01132 human GSE8157 sample 2796	12/269	2.70×10^{-07}	7.17×10^{-07}
tibolone 444008 human GSE12446 sample 3204	35/313	4.90×10^{-33}	8.68×10^{-32}

Since it is unlikely that this level of agreement is purely accidental, the drugs identified in the present study can be useful candidates for further evaluation in COVID-19 therapy. This work therefore provides a foundation for further research pertaining to utilizing advanced learning concepts to analyze COVID-19 infectious disease.

ACKNOWLEDGMENT

This study was supported by KAKENHI grants 19H05270, 20H04848, and 20K12067. This project was also funded by the Deanship of Scientific Research (DSR) at King Abdulaziz University, Jeddah, under grant no. KEP-8-611-38. The authors, therefore, acknowledge DSR with thanks for providing technical and financial support.

REFERENCES

[1] S. Pfaender, K. B. Mar, E. Michailidis, A. Kratzel, D. Hirt, P. V'kovski, W. Fan, N. Ebert, H. Stalder, H. Kleine-Weber, M. Hoffmann, H. H. Hoffmann, M. Saeed, R. Dijkman, E. Steinmann, M. Wight-Carter, N. W. Hanners, S. Pöhlmann, T. Gallagher, D. Todt, G. Zimmer, C. M. Rice, J. W. Schoggins, and V. Thiel, "Ly6e impairs coronavirus fusion and confers immune control of viral disease," *bioRxiv*, 2020. [Online]. Available: https://www.biorxiv.org/content/early/2020/03/07/2020.03.05.979260

[2] Y. h. Taguchi, *Unsupervised feture extraction applied to bioinformatics: PCA and TD based approach*. Switzerland: Springer International, 2020.

[3] M. V. Kuleshov, M. R. Jones, A. D. Rouillard, N. F. Fernandez, Q. Duan, Z. Wang, S. Koplev, S. L. Jenkins, K. M. Jagodnik, A. Lachmann, M. G. McDermott, C. D. Monteiro, G. W. Gundersen, and A. Ma'ayan, "Enrichr: a comprehensive gene set enrichment analysis web server 2016 update," *Nucleic Acids Research*, vol. 44, no. W1, pp. W90–W97, 05 2016. [Online]. Available: https://doi.org/10.1093/nar/gkw377

[4] Y. Zhou, B. Zhou, L. Pache, M. Chang, A. H. Khodabakhshi, O. Tanaseichuk, C. Benner, and S. K. Chanda, "Metascape provides a biologist-oriented resource for the analysis of systems-level datasets," *Nature Communications*, vol. 10, no. 1, apr 2019. [Online]. Available: https://doi.org/10.1038/s41467-019-09234-6

[5] P. C. Woo, Y. Huang, S. K. Lau, H.-w. Tsoi, and K.-y. Yuen, "In silico analysis of orf1ab in coronavirus hku1 genome reveals a unique putative cleavage site of coronavirus hku1 3c-like protease," *Microbiology and Immunology*, vol. 49, no. 10, pp. 899–908, 2005. [Online]. Available: https://onlinelibrary.wiley.com/doi/abs/10.1111/j.1348-0421.2005.tb03681.x

[6] M. Hoffmann, H. Kleine-Weber, S. Schroeder, N. Krüger, T. Herrler, S. Erichsen, T. S. Schiergens, G. Herrler, N.-H. Wu, A. Nitsche, M. A. Müller, C. Drosten, and S. pöhlmann, "Sars-cov-2 cell entry depends on ace2 and tmprss2 and is blocked by a clinically proven protease inhibitor," *Cell*, vol. 181, no. 2, pp. 271 – 280.e8, 2020. [Online]. Available: http://www.sciencedirect.com/science/article/pii/S0092867420302294

[7] S. Matsuyama, N. Nao, K. Shirato, M. Kawase, S. Saito, I. Takayama, N. Nagata, T. Sekizuka, H. Katoh, F. Kato, M. Sakata, M. Tahara, S. Kutsuna, N. Ohmagari, M. Kuroda, T. Suzuki, T. Kageyama, and M. Takeda, "Enhanced isolation of sars-cov-2 by tmprss2-expressing cells," *Proceedings of the National Academy of Sciences*, vol. 117, no. 13, pp. 7001–7003, 2020. [Online]. Available: https://www.pnas.org/content/117/13/7001

[8] T. H. Bugge, T. M. Antalis, and Q. Wu, "Type ii transmembrane serine proteases," *Journal of Biological Chemistry*, vol. 284, no. 35, pp. 23 177–23 181, 2009. [Online]. Available: http://www.jbc.org/content/284/35/23177.abstract

TABLE IX
LIST OF *in silico* SCREENED DRUGS [21] WHOSE TARGET GENES ARE ALSO ENRICHED IN THE 134 GENES SELECTED BY TD BASED UNSUPERVISED FE.

Term	Overlap	P-value	Adjusted P-value
Drug Perturbations from GEO up			
quercetin DB04216 mouse GSE38141 sample 3435	33/280	6.85×10^{-32}	6.74×10^{-31}
quercetin DB04216 mouse GSE38136 sample 3438	31/254	1.99×10^{-30}	1.80×10^{-29}
quercetin DB04216 mouse GSE38136 sample 3437	37/472	2.85×10^{-29}	2.37×10^{-28}
quercetin 5280343 rat GSE7479 sample 3409	33/394	5.47×10^{-27}	3.97×10^{-26}
quercetin DB04216 mouse GSE38136 sample 3436	30/297	5.97×10^{-27}	4.29×10^{-26}
quercetin DB04216 mouse GSE38067 sample 3440	26/227	8.02×10^{-25}	4.88×10^{-24}
quercetin 5280343 human GSE7259 sample 3416	29/327	1.99×10^{-24}	1.17×10^{-23}
quercetin DB04216 mouse GSE38067 sample 3441	20/114	4.34×10^{-23}	2.37×10^{-22}
quercetin 5280343 human GSE13899 sample 3182	16/307	2.56×10^{-10}	6.85×10^{-10}
quercetin DB04216 mouse GSE4262 sample 3428	14/360	1.42×10^{-07}	3.29×10^{-07}
quercetin DB04216 mouse GSE4262 sample 3429	9/229	2.44×10^{-05}	5.14×10^{-05}
quercetin 5280343 human GSE7259 sample 3415	9/336	4.44×10^{-04}	8.58×10^{-04}
quercetin DB04216 mouse GSE4262 sample 3433	8/323	1.52×10^{-3}	2.82×10^{-3}
quercetin DB04216 mouse GSE4262 sample 3434	8/324	1.55×10^{-3}	2.87×10^{-3}
quercetin DB04216 mouse GSE4262 sample 3431	7/252	1.56×10^{-3}	2.89×10^{-3}
quercetin DB04216 mouse GSE4262 sample 3427	8/360	2.97×10^{-3}	5.40×10^{-3}
quercetin DB04216 mouse GSE4262 sample 3432	5/254	2.83×10^{-3}	4.76×10^{-3}
Drug Perturbations from GEO down			
quercetin DB04216 mouse GSE38067 sample 3441	59/486	1.81×10^{-59}	8.19×10^{-57}
quercetin DB04216 mouse GSE38136 sample 3437	26/128	$1.33 \times 10^{-3}1$	2.00×10^{-30}
quercetin 5280343 human GSE7259 sample 3415	29/264	4.05×10^{-27}	4.57×10^{-26}
quercetin DB04216 mouse GSE38136 sample 3436	30/303	1.09×10^{-26}	1.17×10^{-25}
quercetin 5280343 human GSE13899 sample 3182	26/293	6.10×10^{-22}	4.55×10^{-21}
quercetin DB04216 mouse GSE38067 sample 3440	28/373	1.31×10^{-21}	9.44×10^{-21}
quercetin DB04216 mouse GSE38136 sample 3438	27/346	2.71×10^{-21}	1.91×10^{-20}
quercetin DB04216 mouse GSE38141 sample 3435	22/320	2.68×10^{-16}	1.26×10^{-15}
quercetin 5280343 human GSE7259 sample 3416	18/273	3.44×10^{-13}	1.36×10^{-12}
quercetin 5280343 rat GSE7479 sample 3409	14/206	1.12×10^{-10}	3.81×10^{-10}
quercetin DB04216 mouse GSE4262 sample 3431	11/348	2.31×10^{-05}	5.47×10^{-05}
quercetin DB04216 mouse GSE4262 sample 3427	5/240	2.28×10^{-3}	4.21×10^{-3}

[9] Y. h. Taguchi* and T. Turki, "Neurological disorder drug discovery from gene expression with tensor decomposition," *Current Pharmaceutical Design*, vol. 25, no. 43, pp. 4589–4599, 2019. [Online]. Available: http://www.eurekaselect.com/node/177329/article

[10] J. R. Burdick and D. P. Durand, "Primaquine diphosphate: Inhibition of newcastle disease virus replication," *Antimicrobial Agents and Chemotherapy*, vol. 6, no. 4, pp. 460–464, 1974. [Online]. Available: https://aac.asm.org/content/6/4/460

[11] D. C. CULITA1, R. ALEXANDROVA, L. DYAKOVA, G. MARINESCU, L. PATRON, R. KALFIN, and M. ALEXANDROV, "Evaluation of cytotoxic and antiproliferative activity of co(ii), ni(ii), cu(ii) and zn(ii) complexes with meloxicam on virus – transformed tumor cells daniela," *Revista de Chimie*, vol. 63, no. 4, pp. 384–389, 2012.

[12] H. E. Renis, "Antiviral activity of cytarabine in herpesvirus–infected rats," *Antimicrobial Agents and Chemotherapy*, vol. 4, no. 4, pp. 439–444, 1973. [Online]. Available: https://aac.asm.org/content/4/4/439

[13] K. Ueda, R. Kawabata, T. Irie, Y. Nakai, Y. Tohya, and T. Sakaguchi, "Inactivation of pathogenic viruses by plant-derived tannins: Strong effects of extracts from persimmon (diospyros kaki) on a broad range of viruses," *PLOS ONE*, vol. 8, no. 1, pp. 1–10, 01 2013. [Online]. Available: https://doi.org/10.1371/journal.pone.0055343

[14] R. Li, R. Narita, R. Ouda, C. Kimura, H. Nishimura, M. Yatagai, T. Fujita, and T. Watanabe, "Structure-dependent antiviral activity of catechol derivatives in pyroligneous acid against the encephalomycarditis virus," *RSC Adv.*, vol. 8, pp. 35 888–35 896, 2018. [Online]. Available: http://dx.doi.org/10.1039/C8RA07096B

[15] P. E. Lobert, D. Hober, A. S. Delannoy, and P. Wattré, "Evidence that neomycin inhibits human cytomegalovirus infection of fibroblasts," *Archives of Virology*, vol. 141, no. 8, pp. 1453–1462, aug 1996. [Online]. Available: https://doi.org/10.1007/bf01718247

[16] H. M. Abuohashish, M. M. Ahmed, D. Sabry, M. M. Khattab, and S. S. Al-Rejaie, "Ace-2/ang1-7/mas cascade mediates ace inhibitor, captopril, protective effects in estrogen-deficient osteoporotic rats," *Biomedicine & Pharmacotherapy*, vol. 92, pp. 58 – 68, 2017. [Online]. Available: http://www.sciencedirect.com/science/article/pii/S0753332217311873

[17] W. Cheng, C. Song, K. M. Anjum, M. Chen, D. Li, H. Zhou, W. Wang, and J. Chen, "Coenzyme q plays opposing roles on bacteria/fungi and viruses in drosophila innate immunity," *International Journal of Immunogenetics*, vol. 38, no. 4, pp. 331–337, 2011. [Online]. Available: https://onlinelibrary.wiley.com/doi/abs/10.1111/j.1744-313X.2011.01012.x

[18] C. M. Finnegan and R. Blumenthal, "Fenretinide inhibits hiv infection by promoting viral endocytosis," *Antiviral Research*, vol. 69, no. 2, pp. 116 – 123, 2006. [Online]. Available: http://www.sciencedirect.com/science/article/pii/S016635420500241X

[19] C. Wu, Y. Liu, Y. Yang, P. Zhang, W. Zhong, Y. Wang, Q. Wang, Y. Xu, M. Li, X. Li, M. Zheng, L. Chen, and H. Li, "Analysis of therapeutic targets for sars-cov-2 and discovery of potential drugs by computational methods," *Acta Pharmaceutica Sinica B*, 2020. [Online]. Available: http://www.sciencedirect.com/science/article/pii/S2211383520302999

[20] L. Yi, Z. Li, K. Yuan, X. Qu, J. Chen, G. Wang, H. Zhang, H. Luo, L. Zhu, P. Jiang, L. Chen, Y. Shen, M. Luo, G. Zuo, J. Hu, D. Duan, Y. Nie, X. Shi, W. Wang, Y. Han, T. Li, Y. Liu, M. Ding, H. Deng, and X. Xu, "Small molecules blocking the entry of severe acute respiratory syndrome coronavirus into host cells," *Journal of Virology*, vol. 78, no. 20, pp. 11 334–11 339, 2004. [Online]. Available: https://jvi.asm.org/content/78/20/11334

[21] A. Ubani, F. Agwom, N. Y. Shehu, P. Luka, A. Umera, U. Umar, S. Omale, N. E. Nnadi, and J. C. Aguiyi, "Molecular docking analysis of some phytochemicals on two sars-cov-2 targets," *bioRxiv*, 2020. [Online]. Available: https://www.biorxiv.org/content/early/2020/04/01/2020.03.31.017657

[22] C. L. Clouser, S. E. Patterson, and L. M. Mansky, "Exploiting drug repositioning for discovery of a novel hiv combination therapy," *Journal of Virology*, vol. 84, no. 18, pp. 9301–9309, 2010. [Online]. Available: https://jvi.asm.org/content/84/18/9301

[23] K. Fukano, S. Tsukuda, M. Oshima, R. Suzuki, H. Aizaki, M. Ohki, S.-Y. Park, M. Muramatsu, T. Wakita, C. Sureau, Y. Ogasawara, and K. Watashi, "Troglitazone impedes the oligomerization of sodium taurocholate cotransporting polypeptide and entry of hepatitis b virus into hepatocytes," *Frontiers in Microbiology*, vol. 9, p. 3257, 2019. [Online]. Available: https://www.frontiersin.org/article/10.3389/fmicb.2018.03257

[24] O. D. Perez, G. P. Nolan, D. Magda, R. A. Miller, L. A. Herzenberg,

 doi:10.20944/preprints202004.0431.v1

and L. A. Herzenberg, "Motexafin gadolinium (gd-tex) selectively induces apoptosis in hiv-1 infected cd4+ t helper cells," *Proceedings of the National Academy of Sciences*, vol. 99, no. 4, pp. 2270–2274, 2002. [Online]. Available: https://www.pnas.org/content/99/4/2270